American Mineralogist, Volume 93, pages 880–885, 2008

Biogenic vs. abiogenic magnetite nanoparticles: A XMCD study

Claire Carvallo,[1,*] Philippe Sainctavit,[1] Marie-Anne Arrio,[1] Nicolas Menguy,[1] Yuheng Wang,[1] Georges Ona-Nguema,[1] and Sandrine Brice-Profeta[1,2]

[1]Institut de Minéralogie et de Physique des Milieux Condensés, Campus Boucicaut, 140 rue de Lourmel, 75015 Paris, France
[2]ENSEEG/LTPCM, Domaine Universitaire 1130 rue de la piscine, BP 7538402 Saint-Martin d'Hères Cedex, France

Abstract

X-ray magnetic circular dichroism (XMCD) experiments were carried out to compare the Fe^{2+}/Fe^{3+} ratio in nanomagnetite chemically produced from lepidocrocite and nanomagnetite biogenically produced by the Fe-reducing bacterium *Shewanella putrefaciens*. Together with TEM imaging, these measurements showed that the biotic magnetite nanoparticles were of excellent quality, with small size dispersion and high crystallinity. From the XMCD measurements, it could be shown that the biogenic nanomagnetite contained a higher amount of Fe^{2+} than the abiogenic nanomagnetite.

Keywords: Nanomagnetite, XMCD, *Shewanella putrefaciens*, biomineralization

Introduction

Iron-respiring bacteria (IRB) have distinct properties that can be used in several fields. They can convert ferrihydrite (Lovley et al. 1987) or lepidocrocite (Cooper et al. 2000; Ona-Nguema et al. 2002a, 2002b) into the magnetic spinel magnetite. Other industrial applications are related to soil remediation where IRB can induce precipitation of heavy metal pollutants such as uranium. The biotechnological potential of IRB lies in their ability to produce nanocrystalline magnetic particles suitable for use with information storage technologies. This would provide low-energy, environmentally friendly processing methodologies (Pattrick et al. 2002). Some bacteria are able to orient and migrate along the magnetic field toward favorable habitats (Blakemore 1975; Bazylinski and Frankel 2004). In environmental magnetism, fossil magnetotactic bacteria can significantly contribute to the magnetic properties of some sediments and soils (Chang and Kirschvink 1989). They are also novel sources for fundamental studies in fine-grain magnetism and magnetic materials. Finally, fossil magnetosome chains could be a suitable biomarker for the presence of life on Earth and other planets (McKay et al. 1996). In this work, we used the spectroscopic technique X-ray magnetic circular dichroism (XMCD) (Sainctavit et al. 2003) to study and compare the compositions of magnetite having two different origins. The first one was produced by Fe(III)-reducing activity, whereas the second one was obtained by an aqueous chemical route.

Samples

The biogenic magnetite was prepared upon the reduction of lepidocrocite (γ-FeOOH) by an IRB, *Shewanella putrefaciens* CIP 59.28 (equivalent to strain ATCC 12099). Bioreduction experiments were performed with 2×10^9 CFU/mL of *S. putrefaciens* at 30 °C with an initial pH of 7.5, in the presence of 110 m*M* of sodium methanoate ($NaHCO_2$) as an electron donor, and 582 m*M* equivalent Fe of γ-FeOOH in a defined mineral medium based on that used by Ona-Nguema et al. (2002a). The 100 μ*M* of anthraquinone-2, 6-disulfonate (AQDS), an electron shuttle, were added in the media to enhance the bacterial reduction of lepidocrocite. After two days of incubation, the formation of magnetite occurred via the transformation of a mixture of hydroxycarbonate green rust and unreduced lepidocrocite. The biogenic magnetite formed under these conditions was characterized by X-ray diffraction (Appendix Fig. 1; note that Appendix Figs. 2 and 3, with supporting text, are also available[1]).

The abiogenic magnetite production was performed in an atmosphere-controlled JACOMEX glove box. All reagents were chemical grade and the solutions were prepared by N_2-purged and deionized H_2O stocked in the glove box. Samples were prepared by neutralizing aqueous Fe^{2+} and lepidocrocite suspension. The 2.81 mL of $FeCl_2$ solution (1 *M*) were added to a serum bottle containing a suspension of 0.5 g lepidocrocite and 91.19 mL N_2-purged and deionized H_2O. Then 6 mL NaOH solution (1 *M*) was injected into the medium, which triggered the formation of abiogenic magnetite. The total volume of the medium was 100 mL and the ionic strength was 0.1162 *M*. The magnetite thus formed was characterized by X-ray diffraction (Appendix Fig. 1[1]).

The biogenic and abiogenic magnetite nanoparticles were preserved in hermetically sealed bottles from which the samples

* E-mail: claire.carvallo@impmc.jussieu.fr

[1]Deposit item AM-08-024, Appendix Figures 1, 2, and 3. Deposit items are available two ways: For a paper copy contact the Business Office of the Mineralogical Society of America (see inside front cover of recent issue) for price information. For an electronic copy visit the MSA web site at http://www.minsocam.org, go to the American Mineralogist Contents, find the table of contents for the specific volume/issue wanted, and then click on the deposit link there.

were extracted by a syringe.

Synthesized magnetite particles were characterized by X-ray diffraction (Rietveld 1969; Langford et al. 2000). To avoid the oxidation by air, each sample powder was placed into a 0.5 mm diameter glass capillary, and sealed with a Superglue stick under N_2 atmosphere in the glove box ($O_2 \leq 20$ ppm). XRD measurements were performed with Co*K* radiation on a Panalytical X'Pert Pro MPD diffractometer mounted in Debye-Scherrer configuration. X-ray powder diffraction patterns were analyzed by the Rietveld method using the XND 1.3 program (Bérar and Baldinozzi 1998). For the samples studied, the line shape was found to be an almost pure Lorentzian profile, dominated by crystal size broadening.

Room-temperature hysteresis curves were measured to characterize the magnetic grain size. Measurements were carried out on a Princeton Measurements Alternating Gradient Magnetometer at the Laboratoire des Sciences du Climat et de l'Environnement in Gif-sur-Yvette, France, with a saturating field of 0.5 T. At room temperature, most of the grains were not blocked and behaved as superparamagnetic (SP) particles (Fig. 1). However, a fraction was in a stable single-domain (SSD) state as shown by the ratio of remnant saturation magnetization over the saturation magnetization (M_{rs}/M_s), which is not null. Indeed, M_{rs}/M_s was 0.14 ± 0.03 for the biogenic sample and 0.16 ± 0.02 for the abiogenic sample. The coercivity fields were 4.7 ± 0.5 and 7.4 ± 0.5 mT for the biogenic and abiogenic samples, respectively. Both samples were saturated at 0.3 T. It was impossible to find any differences between the two samples based on their hysteresis loops alone.

Experimental methods

High-resolution transmission electron microscope (HR-TEM) observations were performed on a JEOL 2100F microscope operating at 200 kV and equipped with a field-emission gun, a high-resolution UHR pole piece, and a Gatan GIF 2001 energy filter. A drop containing the magnetite particles, previously sonicated for 10 min, was deposited onto a carbon-coated 200 mesh copper grid. The excess of water was removed with an absorbing paper and the remaining water was pumped in the airlock chamber of the microscope.

The XMCD spectra were recorded on the SIM beam line of the Swiss Light Source. The X-ray source is a tunable Apple II undulator providing a high flux of circular polarized photons (Sasaki 1994). The SLS ring operates at 2.4 GeV and we have been using the fundamental peak of the source with 100% circular polarization. The beam is monochromatized by an SX-700 type plane-grating monochromator with an estimated instrumental resolution of 0.120 eV at 750 eV. The XMCD end-station is an ultra high-vacuum vessel where a sample can be cooled down to any temperature between 300 and 1.5 K and magnetized by a superconducting coil delivering a magnetic induction between 0 and ±7 T. The incoming photon flux and the absorbed photon flux were monitored by Total Electron Yield measured in the current mode by Keithley electrometers. The XMCD spectra were acquired in the following way. An external magnetic field was applied and spectra were measured with left helicity. Then the helicity was switched to right and back to left several times until a good signal-to-noise ratio was obtained. In a second step, the same procedure was performed again with the opposite magnetic direction for the external magnetic field. This procedure ensured a high signal-to-noise ratio and allowed us to discard any spurious systematic signals. All the XMCD spectra have been measured for samples cooled to 200 K and in an external magnetic field of 2 T.

Magnetite contains divalent iron and can be oxidized into maghemite (γ-Fe_2O_3) by exposure to air. The sample preparation was optimized so that no such extra oxidation occurred. Several sets of X-ray absorption spectroscopy (XAS) measurements were necessary to determine the best sample preparation. We first started with a preparation in a glove box that was directly connected to the airlock chamber of the XMCD set-up. This complicated and awkward procedure gave us some reference spectra. In a second experiment, we simplified the procedure and prepared the samples by drop casting the magnetite directly on the sample holder in a nitrogen atmosphere. In this second preparation mode, the drop was efficiently dried in the pumped airlock chamber. It was found that this second preparation mode yielded the same type of results as the one obtained from the glove box samples (Appendix Fig. 1[1]). All the samples reported below were prepared by direct drop casting the magnetite in the air-lock chamber.

Multiplets

To extract quantitative information, the XAS and XMCD spectra at the Fe $L_{2,3}$ edges were simulated using ligand field multiplet (LFM) calculations developed by Theo Thole (de Groot et al. 1990). The details can be found in Cowan (1981), Butler (1981), Thole et al. (1985), and Arrio et al. (1996). Fe $L_{2,3}$ edges consist mainly of electric dipole-allowed $2p^63d^5 \rightarrow 2p^53d^6$ $2p \rightarrow 3d$ transitions, as the dipole-allowed $2p^64s^0 \rightarrow 2p^54d^1$ $2p \rightarrow 4s$ transitions have a negligible contribution to the absorption cross-section. For clarity, we describe the calculation process for Fe^{3+}, i.e., $2p^63d^5$ ground state configuration. In spherical symmetry, the $2p^63d^5$ ground state and the $2p^53d^6$ excited state energy levels are split by the interelectronic repulsions and the spin-orbit coupling. The radial integrals for interelectronic repulsions and spin-orbit coupling were calculated using the atomic Hartree-Fock code of Cowan (1981). One had to take into account for the initial $2p^63d^5$ configuration, the direct $F^2(3d, 3d)$ and $F^4(3d, 3d)$ Slater integrals and the 3d shell spin-orbit coupling parameter ζ_{3d} and the excited $2p^53d^6$ configuration, the direct $F^2(3d, 3d)$, $F^4(3d, 3d)$, and $F^2(2p, 3d)$ Slater integrals, the exchange $G^1(2p, 3d)$, $G^3(2p, 3d)$ Slater integrals, ζ_{3d}, and the 2p shell spin-orbit coupling ζ_{2p}. The Slater integrals

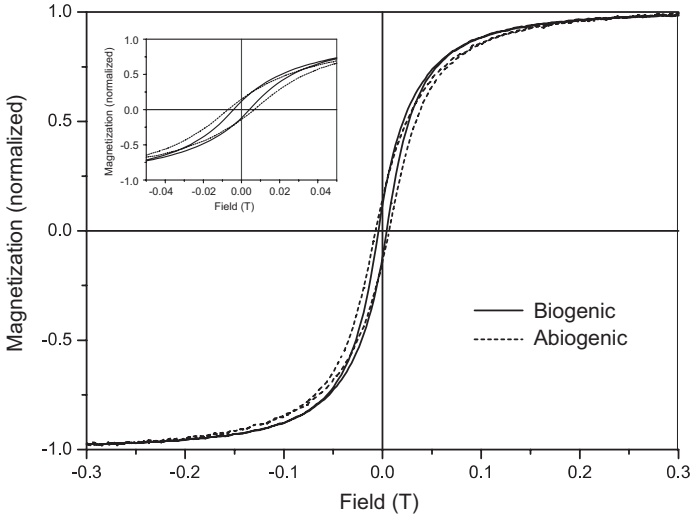

Figure 1. Room-temperature hysteresis loops for biogenic and abiogenic magnetite nanoparticles measured in a saturating field of 0.5 T at room temperature. Inset: detail of the inside of the loops.

were reduced using the κ parameter. This reduction accounted for the electronic delocalization occurring through the chemical bonding in the solid. The effect of the crystal field and of the local magnetic field at the absorbing atom was treated using the group subduction of Butler (1981). For octahedral and tetrahedral sites of the spinel structure, the O_3-O_h and the O_3-T_d branchings were used. The crystal field was then described by a single parameter, 10 Dq. The local magnetic field appears in the Zeeman hamiltonian: $H_{Zee} = g\,\mu_B\,H\,Sz$. In ferro- and ferrimagnetic oxides, the $g\,\mu_B H$ parameter may typically range from 5 to 100 meV (van der Laan and Thole 1991). The intensities of the transitions were calculated in the electric dipole approximation. To simulate the experimental XAS spectra and XMCD signals, the transition lines for all cross-sections were broadened by a Lorentzian function to account for the core-hole lifetime, and by a Gaussian function to account for instrumental resolution. The width of the Lorentzian was 0.3 eV for the part of the spectrum between 700 and 720 eV, and 0.4 eV for the part between 720 and 740 eV. The width of the Gaussian was 0.3 eV.

Results

The shape and crystallinity of the biogenic and abiogenic magnetite particles were measured by HR-TEM. The local magnetic properties were registered with XMCD at the Fe $L_{2,3}$ edges.

XRD results showed that biogenic and abiogenic magnetite particles have almost the same average size (31.0 ± 7.2 nm for the biogenic ones and 22.5 ± 12.5 nm for the abiogenic ones). HR-TEM observations were consistent with these measurements. Moreover, as shown in Figure 2, the biogenic magnetite particles have an octahedral shape, whereas the abiotic magnetite particles have an undefined spheroidal shape. A careful examination of HR-TEM images of both biogenic and abiotic magnetite particles failed to reveal the presence of defects or any significant difference in crystal perfection.

The Fe $L_{2,3}$ edges of the isotropic spectra for the biogenic and abiogenic magnetite particles are reported in Figure 3. The two spectra are similar except for a small shoulder on the L_3 edge at 712 eV. The general shapes of the two spectra are in line with those already published (Chen et al. 1990; Goering et al. 2006; Pearce et al. 2006). The isotropic spectra represent the averaged sum of the spectra for the two directions of the magnetic field and the right and left helicities. The measurements were repeated several times to check for the reproducibility of the experimental features. Since the samples are randomly oriented nanocrystals with cubic symmetry, it can be shown that the average $(\sigma_{Right}-\sigma_{Left})/2$ is almost equal to the isotropic cross-section (i.e., for such samples there is no X-ray magnetic linear dichroism). The two isotropic spectra have been normalized to 1 at the maximum of the L_3 edge.

The XMCD spectra for the biogenic and abiogenic magnetite particles are reported in Figure 4. Again the two spectra are quite similar to each other and in line with those previously published (Chen et al. 1990; Goering et al. 2006; Pearce et al. 2006). The XMCD spectra are raw difference spectra without any treatment such as background subtraction or normalization coefficient except for the isotropic normalization previously described. The

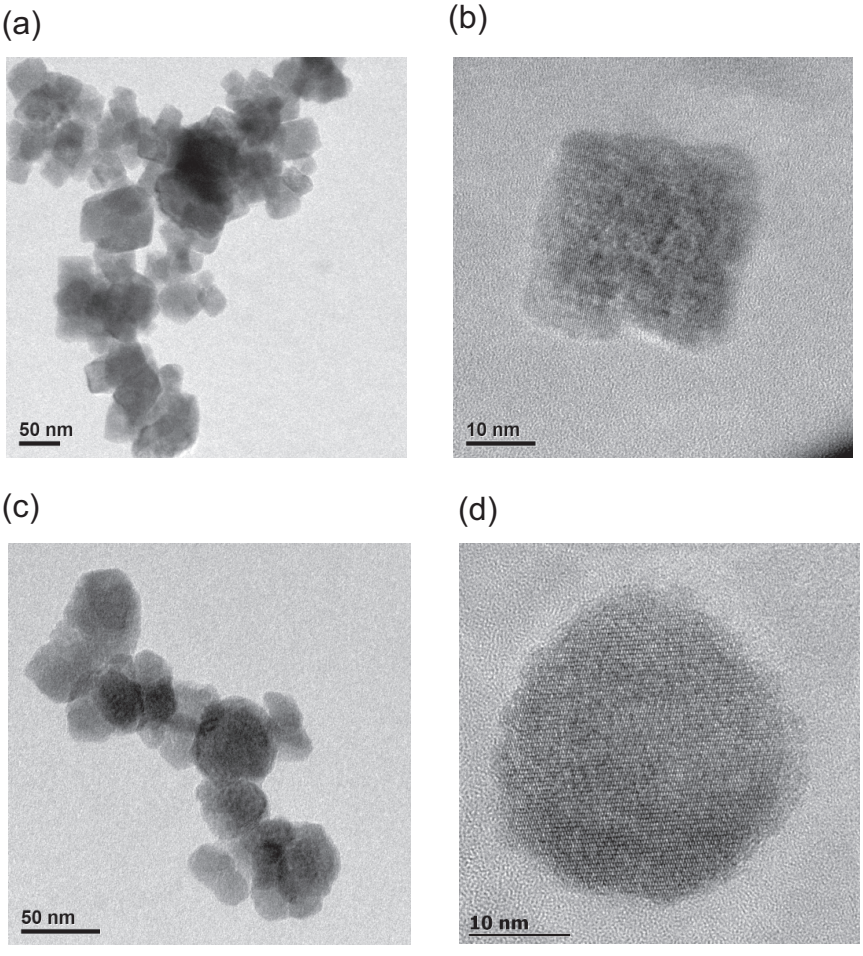

Figure 2. HR-TEM images of (**a**) magnetite obtained upon anaerobic reduction of lepidocrocite by *Shewanella putrefaciens*; (**b**) octahedral crystal of biogenic magnetite; (**c**) abiogenic magnetite produced from lepidocrocite. (**d**) Single crystal of abiogenic magnetite.

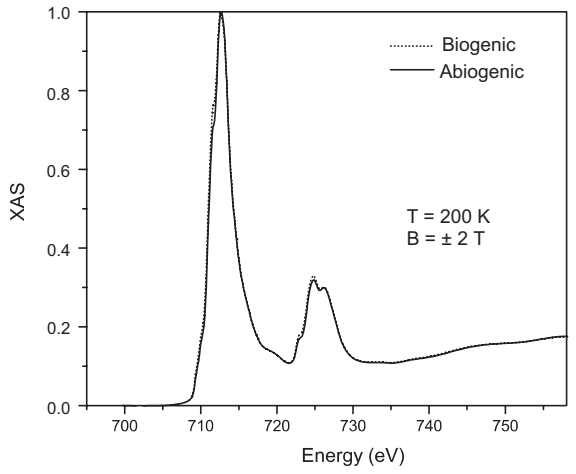

FIGURE 3. XAS spectra measured on biogenic (dotted line) and abiogenic (solid line) magnetite nanoparticles at Fe $L_{2,3}$ edges. The temperature is 200 K and the external magnetic field is 2 T.

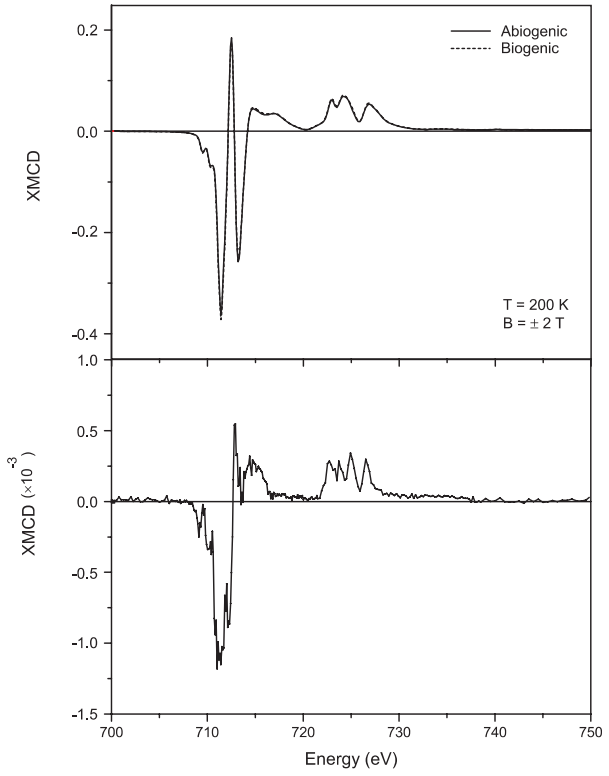

FIGURE 4. Upper panel: XMCD spectra measured on biogenic and abiogenic magnetite nanoparticles at Fe $L_{2,3}$ edges. Lower panel: difference of the two XMCD signals. Note that the vertical scales for the two panels are different.

XMCD spectra are the sum of four series where a series stands for the four spectra with the two photon helicities and the two field directions.

To understand the experimental spectra, we performed multiplet calculations with the set of parameters chosen in Brice-Profeta et al. (2005) for the Fe^{3+} ions in maghemite and the set of parameters in Brice-Profeta (2004) for Fe^{2+} (κ = 60%, ζ_{2p} = 8.35 eV, ζ_{3d} = 0.01 eV, 10 Dq = 1.4 eV). The average energy of the $2p^53d^{n+1}$ configuration is 714.57 eV for Fe^{2+} and 715.46 eV for Fe^{3+}. The Fe^{2+} average energy was expected to be around 714.5 eV due to the chemical shift between Fe^{2+} and Fe^{3+} and was optimized by comparison with XAS and XMCD signals. It has to be noted that the same parameters have been used for the ground and excited configurations. All the cross-sections have been calculated in the electric-dipole approximation for a cubic (octahedral or tetrahedral) crystallographic environment. In the upper part of Figure 5, we report the three isotropic spectra for a octahedral Fe^{2+}, tetrahedral Fe^{3+}, and octahedral Fe^{3+}. The lower part represents the XMCD spectra for the three types of iron ions where the antiferromagnetic coupling between the tetrahedral and the octahedral sub-networks has been considered. From this figure, the origin of the various features of the experimental XMCD signal can already be interpreted. The first negative peak (A) comes mainly from octahedral Fe^{3+} with an extra contribution from octahedral Fe^{3+}. The positive peak (B) comes from tetrahedral Fe^{3+} and the negative peak (C) from octahedral Fe^{3+}. The XMCD signal at the L_2 edge cannot be easily separated into its various contributions since the contributions of each ion is broad and superimposed upon each other.

To check the goodness of the calculations, the calculated and XMCD signal for magnetite have been compared to the isotropic and XMCD experimental signals of the biogenic magnetite (Fig. 6). The fair agreement between calculations and experiments for this magnetite is an indication of the correct interpretation of the experimental signals. It should be noted that the agreement between the calculation and the experiment is not good in the energy region extending from 715 to 720 eV. This is true for the isotropic spectra where a large, featureless transition is missing, and this is even more clearly visible on the XMCD signal. This discrepancy is well known and generally attributed to the Fe-ligand charge transfer with the creation of a partial ligand-hole due to sigma-bonding. This can be corrected by the use of Configuration Interaction, which is a sound route when the absorbing ion is present in only one valence state and in only one site (Arrio et al. 1996). This is clearly not the case for magnetite and in such complicated compounds, we have to stick to a single configuration approach.

Our interest mainly resides in understanding the differences between the two types of magnetite. Though the two types of magnetite are very similar, the Ligand Field Multiplet calculations and the excellent signal-to-noise ratio with which the XMCD spectra have been collected allow us to extract a reliable difference signal. We have checked by comparison with various series that the difference signal presented in Figure 4 was indeed highly reproducible. The signal is small and amounts to around 5% of the maximum XMCD signal. The maximum of the XMCD difference is around 712 eV. It must be noticed that the unavoidable spurious difference signal between two measurements of the same sample, is measured to be around 0.9%. Thus, it can be safely stated that the difference signal between biogenic and abiogenic XMCD spectra is larger than any systematic instrumental error.

Moreover, the shape of the difference signal is much different from a derivative signal and also much different from the XMCD itself so that energy stability of the beamline and bad

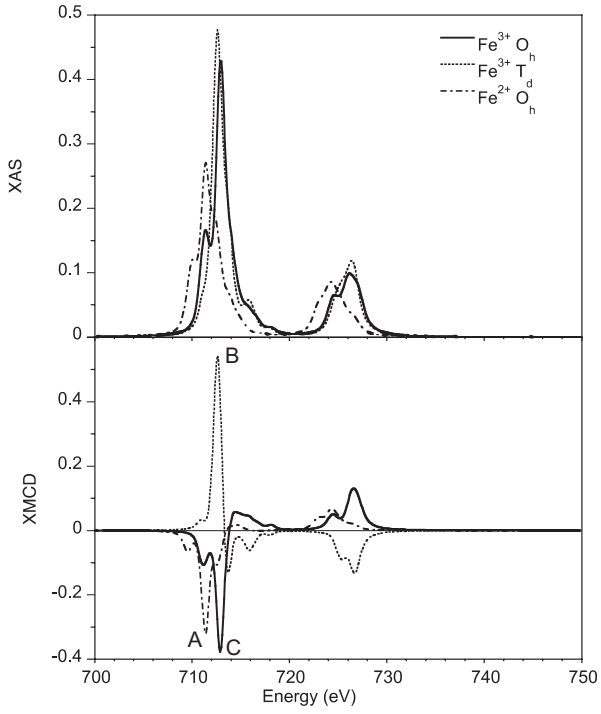

FIGURE 5. XAS spectra (upper panel) and XMCD spectra (lower panel) at Fe $L_{2,3}$ edges in magnetite calculated in the Ligand Field Multiplet theory.

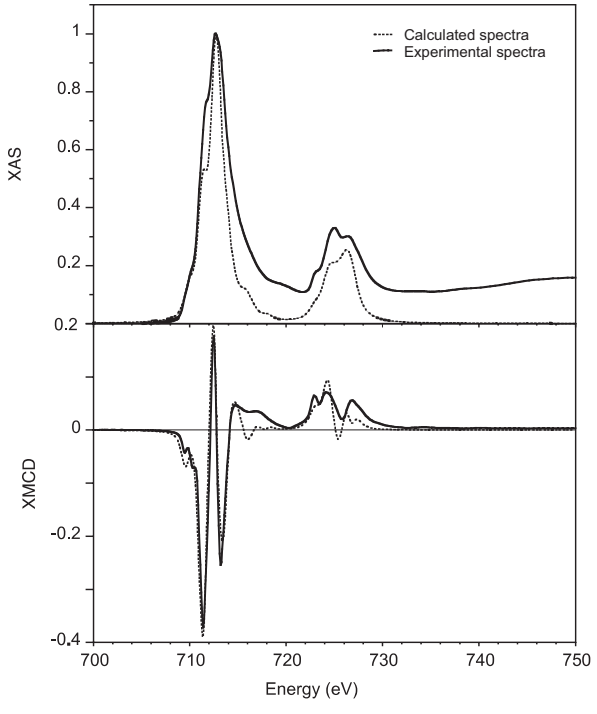

FIGURE 6. Comparison between the calculated (dotted line) and experimental (biogenic, solid line) spectra. Top: isotropic XAS spectra; bottom: XMCD spectra. Dotted line: calculated spectra; solid line: experimental spectra.

normalization cannot be invoked to explain the data. Starting from the fair agreement between multiplet calculations and experimental XMCD, the difference signal between the two XMCD spectra could be modeled by a linear combination of the three Fe contributions: $Fe^{2+}(O_h)$, $Fe^{3+}(T_d)$, and $Fe^{3+}(O_h)$. The difference signal could be fairly well simulated by a 4.5% contribution from $Fe^{2+}(O_h)$ minus a 3% contribution from $Fe^{3+}(O_h)$ and 1.5% contribution of $Fe^{3+}(T_d)$ (Fig. 7). The agreement is fair and the simulation is mainly intended to give a general idea of the magnetic differences between the biogenic and the abiogenic magnetite particles. One should notice that the charge equilibrium on the octahedral lattice is satisfied and that the extra 1.5% contribution of $Fe^{3+}(T_d)$ corresponds to the vacancies associated to the partial oxidation of the abiogenic magnetite. It should be noted that the agreement is poor in the energy region between 715 and 720 eV. This could be expected from the above-mentioned poor agreement in the same region for both isotropic and XMCD signals.

The interpretation that can be given to the simulation is the following. Both biogenic and abiogenic types of magnetite are quite similar with an almost (1:1:1) proportion between the magnetic contributions arising from the $Fe^{2+}(O_h)$:$Fe^{3+}(T_d)$:$Fe^{3+}(O_h)$ sites. Nevertheless, the high signal-to-noise ratio allows us to conclude that the abiogenic magnetite contains a slightly smaller amount of Fe^{2+} in octahedral sites. This is compensated by a slight increase in the occupancy of the octahedral sites by Fe^{3+}. The abiogenic magnetite is slightly oxidized, or closer to maghemite, as compared to the biogenic sample. From the numerical analysis in Figure 7, the abiogenic magnetite particles can be said to be equivalent to 96 ± 1 wt% pure magnetite (Fe_3O_4) and 4 ± 1 wt% pure maghemite ($Fe_{8/3}O_4$). Since both biogenic and abiogenic magnetite particles were synthesized in similar oxygen-free conditions, the partial oxidation of the abiogenic ones could come from a larger disorder on the octahedral sub-network allowing the appearance of a small amount of vacancies (less than 1% of the spinel octahedral sites) compensated by a variation of the $Fe^{2+}(O_h)$:$Fe^{3+}(O_h)$ ratio. These results are consistent with the study of Coker et al. (2007), who found with XMCD measurements that chemically synthesized nanomagnetite is more oxidized than intracellular nanoscale magnetite produced

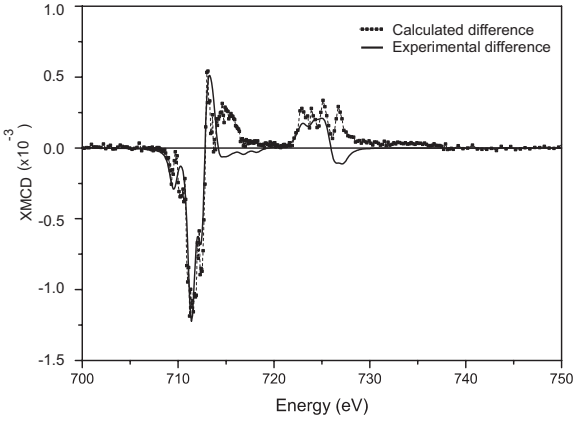

FIGURE 7. LFM analysis of the difference between biogenic and abiogenic XMCD signals (solid line) compared with the experimental signal (dotted line).

by magnetotactic bacteria.

Fe^{2+}-excess magnetite particles have been reported in several studies (e.g., Tamaura and Tahata 1990; Kukkadapu et al. 2005). Their Fe^{2+}/Fe_{TOT} ratio can vary between 0.4 and 0.6. As our results are consistent with these studies, the alternative explanations expressed in these earlier works bear consideration.

A comparison between the magnetite nanoparticles synthesized by *Shewanella putrefaciens* and those obtained by pure chemical synthesis showed that the biogenic magnetite nanoparticles were of excellent quality, with a small size dispersion and a high crystallinity. From the XMCD measurements, it could be shown that the biogenic nanomagnetite contains a higher amount of Fe^{2+} than the abiogenic nanomagnetite. The high crystallinity and the high amount of Fe^{2+} is often considered as a sign of biogenic nanomagnetite with an intracellular origin such as those produced by *Magnetospirillum gryphiswaldense* or *Aquaspirillum magnetotacticum*. The exceptional reducing power of *Shewanella putrefaciens* probably explains the high $Fe^{2+}(O_h)$ concentration. Bacteria such as *Shewanella putrefaciens* are likely to be good candidates for industrial applications where well-crystallized, stoechiometric magnetite nanoparticles are needed.

Acknowledgments

We are glad to acknowledge the instrumental help from Fritjhof Nolting on the SIM beamline and the SLS staff for operating the synchrotron. The nanoparticles have been synthesized within the laboratory facilities developed by Guillaume Morin who contributed to this piece of work by his stimulating discussions. The multiplet calculations were performed with the TT-Multiplet package developed by Theo Thole. We thank Carlo Laj and Catherine Kissel for access to the Alternating Field Magnetometer in the Laboratoire des Sciences du Climat et de l'Environnement and help with the measurements. We thank Ute Golla-Schindler, Robert Kopp, an anonymous reviewer, and associate editor Joshua Feinberg for constructive review comments that helped to improve the paper.

References cited

Arrio, M.A., Sainctavit, Ph., Cartier dit Moulin, C., Mallah, M., Verdaguer, M., Pellegrin, E., and Chen, C.T. (1996) Characterization of chemical bonds in bimetallic cyanides using X-ray absorption spectroscopy at $L_{2,3}$ edges. Journal of American Chemical Society, 118, 6422–6427.

Bazylinski, D.A. and Frankel, R.B. (2004) Magnetosome formation in Prokaryotes. Nature Reviews in Microbiology, 2, 217–230.

Bérar, J.F. and Baldinozzi, G. (1998) XND code: From X-ray laboratory data to incommensurately modulated phases. Rietveld modeling of complex materials. CPD Newsletter, 20, 3–5 (http://www.ccp14.ac.uk).

Blakemore, R.P. (1975) Magnetotactic bacteria. Science, 190, 377–379.

Brice-Profeta, S. (2004) Etude de l'ordre chimique et magnétique d'oxydes spinelles de taille nanométrique par dichroisme magnétique circulaire des rayons X. Ph.D. thesis, Université Paris VI, France.

Brice-Profeta, S., Arrio, M.A., Tronc, E., Menguy, N., Letard, I., Cartier dit Moulin, C., Noguès, M., Chanéac, C., Jolivet, J.P., and Sainctavit, Ph. (2005) Magnetic order in γ-Fe_2O_3 nanoparticles: A XMCD study. Journal of Magnetism and Magnetic Materials, 288, 354–365.

Butler, P.H. (1981) Point group symmetry applications: Methods and tables. Plenum Press, New York.

Chang, S.B.R. and Kirschvink, J.L. (1989) Magnetofossils, the magnetization of sediments and the evolution of magnetite biomineralization. Annual Review of Earth and Planetary Sciences, 17, 169–195.

Chen, C.T., Sette, F., Ma, Y., and Modesti, S. (1990) Soft X-ray magnetic circular dichroism at the $L_{2,3}$ edges of nickel. Physical Review B, 42, 1943–1946.

Coker, V.S., Pearce, C.I., Lang, C., van der Laan, G., Pattrick, R.A.D., Telling, N.D., Schüler, D., Arenholz, E., and Lloyd, J.R. (2007) Cation site occupancy of biogenic magnetite compared to polygenic ferrite spinels determined by X-ray magnetic circular dichroism. European Journal of Mineralogy, 19, 707–716.

Cooper, D.C., Picardal, F., Rivera, J., and Talbot, C. (2000) Zinc immobilization and magnetite formation via ferric oxide reduction by *Shewanella putrefaciens*. Environmental Science and Technology, 34, 100–106.

Cowan, R.D. (1981) The Theory of Atomic Structure and Spectra. Los Alamos series in basic and applied sciences, University of California Press, Berkeley.

de Groot, F.M.F., Fuggle, J.C., Thole, B.T., and Sawatsky, G.A. (1990) $L_{2,3}$ X-ray absorption edges of d^0 compounds: K^+, Ca^{2+}, Sc^{3+}, and Ti^{4+} in O_h (octahedral) symmetry. Physical Review B (Condensed Matter), 41, 928–937.

Goering, E., Gold, S., Lafkioti, M., and Schütz, G. (2006) Vanishing Fe 3d orbital moments in single-crystalline magnetite. Europhysics Letters, 73, 97–103.

Kukkadapu, R.K., Zachara, J.M., Frederickson, J.K., Kennedy, D.W., Dohnalkova, A.C., and McCready, D.E. (2005) Ferrous hydroxy carbonate is a stable transformation product of biogenic magnetite. American Mineralogist, 90, 510–515.

Langford, J.I., Loüer, D., and Scardi, P. (2000) Effect of a crystallite size distribution on X-ray diffraction line profiles and whole-powder-pattern fitting. Journal of Applied Crystallography, 33, 964–974.

Lovley, D.L, Stolz, J.F., Nord Jr., G.L., and Phillips, E.J.P. (1987) Anaerobic production of magnetite by a dissimilatory iron-reducing microorganism. Nature, 330, 252–254.

McKay, D.S., Gibson Jr., E.K., Vali, H., Romanek, C.S., Clemett, S.J., Cilier, X.D.F., Maechling, C.R., and Zare, R.N. (1996) Search for Past Life on Mars: Possible Relic Biogenic in Martian Meteorite ALH84001. Science, 273, 924–930.

Ona-Nguema, G., Abdelmoula, M., Jorand, F., Benali, O., Géhin, A., Block, J.-C., and Génin, J.-M.R. (2002a) Iron (II,III) hydroxycarbonate green rust formation and stabilization from lepidocrocite bioreduction. Environmental Science and Technology, 36, 16–20.

——— (2002b) Microbial reduction of lepidocrocite by *Shewanella putrefaciens*; the formation of a green rust. Hyperfine Interactions, 5, 415–418.

Pattrick, R.A.D., van der Laan, G., Henderson, C.M.B., Kuiper, P., Dudzik, E., and Vaughan, D.J. (2002) Cation site occupancy in spinel ferrites studied by X-ray magnetic circular dichroism: developing a method for mineralogists. European Journal of Mineralogy, 14, 1095.

Pearce, C.I., Henderson C.M.B., Pattrick R.A.D., van der Laan, G., and Vaughan, D.J. (2006) Direct determination of cation site occupancies in natural ferrites spinels by $L_{2,3}$ X-ray absorption spectroscopy and X-ray magnetic circular dichroism. American Mineralogist, 91, 880–893.

Rietveld, H. (1969) A profile refinement method for nuclear and magnetic structures. Journal of Applied Crystallography, 2, 65–71.

Sainctavit, Ph., Cartier dit Moulin, C., and Arrio, M.-A. (2003) Magnetic measurements at the atomic scale in molecular magnetic and paramagnetic compounds. In J.S. Miller and M. Drillon, Eds., Magnetism: Molecules to Materials I, p. 131–153. Wiley-VCH Verlag GmbH and Co., Salt Lake City.

Sasaki, S. (1994) Analyses for a planar variably-polarizing undulator. Nuclear Instruments and Methods A, 347, 83–86.

Tamaura, Y. and Tahata, M. (1990) Complete reduction of carbon dioxide to carbon using cation excess magnetite. Nature, 346, 255–256.

Thole, B.T., van der Laan, G., Fuggle, J.C., Sawatzky, G., Kartnatak, R.C., and Esteva, J.M. (1985) 3d X-ray absorption lines and the $3d^94f^{n+1}$ multiplets of the lanthanides. Physical Review B, 32, 5107–5118.

van der Laan, G. and Thole, B. (1991) Strong magnetic X-ray dichroism in 2*p* absorption spectra of 3*d* transition-metal ions. Physical Review B, 43, 13401–13411.

Manuscript received June 12, 2007
Manuscript accepted December 30, 2007
Manuscript handled by Joshua Feinberg